STAR Highlights and Future

Journal of Physics: Conference Series **1390** (2019) 012020 doi:10.1088/1742-6596/1390/1/012020

STAR Highlights and Future

Grigory Nigmatkulov (for the STAR Collaboration)
National Research Nuclear University MEPhI
115409, Kashirskoe shosse 31, Moscow, Russia

E-mail: ganigmatkulov@mephi.ru; nigmatkulov@gmail.com

Abstract. We present recent results from the STAR experiment at Relativistic Heavy Ion Collider (RHIC): beam-energy dependence of directed flow of identified particles (including open charm hadrons), flow decorrelation, global and local hyperon polarization, femtoscopic measurements, heavy flavour production, jets, and plan for the future upgrades.

1. Introduction

Lattice QCD calculations suggest that the transition from hadronic matter to a Quark-Gluon Plasma (QGP) phase [1] in gold ion collisions at the top Relativistic Heavy Ion Collider (RHIC) energy ($\sqrt{s_{NN}} \approx 200$ GeV), where the baryon chemical potential $\mu_B \approx 0$ MeV, is a smooth crossover [2, 3]. At lower energies (higher μ_B) it is predicted that the transition between these phases may be of the first order [4, 5]. At even higher μ_B, the excited nuclear matter is expected to remain in a hadronic phase throughout the interaction. A beam energy scan (BES) program at RHIC was proposed to further explore the QCD phase diagram, including a search for the critical point, and to demonstrate that signatures for QGP formation turn off at sufficiently low collision energies [6]. The STAR experiment at RHIC is equipped with a Time Projection Chamber (TPC), a Time-of-Flight (TOF) detector, and a Barrel ElectroMagentic Calorimeter (BEMC) for particle detection and identification with full azimuthal coverage at midrapidity ($|\eta| < 1$). At forward and backward rapidities, Beam-Beam Counters (BBC), Vertex Position Detectors (VPD) and Zero-Degree Calorimeters (ZDC) are used to trigger on minimum-bias collisions and for event plane reconstruction. A silicon vertex detector, the Heavy Flavor Tracker (HFT), was installed in STAR and took data in 2014-2016. It provided excellent vertex position and track pointing resolutions, allowing a detailed study of open heavy flavor hadron production at RHIC. In 2016, an electromagnetic calorimeter placed at $2.5 < \eta < 4$, the Forward Meson Spectrometer (FMS), participated in data taking in Au+Au collisions, allowing longitudinal flow decorrelation measurements at RHIC.

In these proceedings, we present recent results from the STAR experiment on beam-energy dependence of directed flow of identified particles (including open charm hadrons), flow decorrelation, global and local hyperon polarization, femtoscopic measurements, heavy flavour production, jets, and plan for the future upgrades.

2. Directed flow

In high-energy heavy-ion collisions, particles are produced with an azimuthally anisotropic momentum distribution, which is a result of the hydrodynamical flow of the QGP. The azimuthal

distribution of emitted particles relative to the so-called flow symmetry planes (event planes) is typically characterized by its Fourier coefficients (v_n):

$$\frac{dN}{d\phi} \propto 1 + 2\sum_{n=1}^{\infty} v_n \cos[n(\phi - \Psi_n)], \tag{1}$$

where ϕ is the azimuthal angle of a produced particle, and Ψ_n is the azimuthal angle of the n^{th}-order event plane [7, 8]. Hydrodynamic calculations [9, 10] have proposed the presence of a minimum in the slope of net-baryon directed flow (e.g. a minimum in the dv_1/dy near midrapidity) versus $\sqrt{s_{NN}}$ as a signature of the first-order phase transition between hadronic matter and QGP. This minimum is related to the softening of the equation of state (EOS). STAR has recently performed directed flow measurements at midrapidity for p, $\bar{p}$, $\pi^{\pm}$ [11] and Λ, $\bar{\Lambda}$, $K^{\pm}$, K^0_s, and ϕ [12] at $\sqrt{s_{NN}}$ = 7.7, 11.5, 14.5, 19.6, 27, 39, 62.4 and 200 GeV in Au+Au collisions. Figure 1(a)(left) shows dv_1/dy slope measurents [12]. Net protons show a minimum in the dv_1/dy in the energy range between $\sqrt{s_{NN}}$ = 11.5 and 19.6 GeV (Fig. 1(b)(left)).

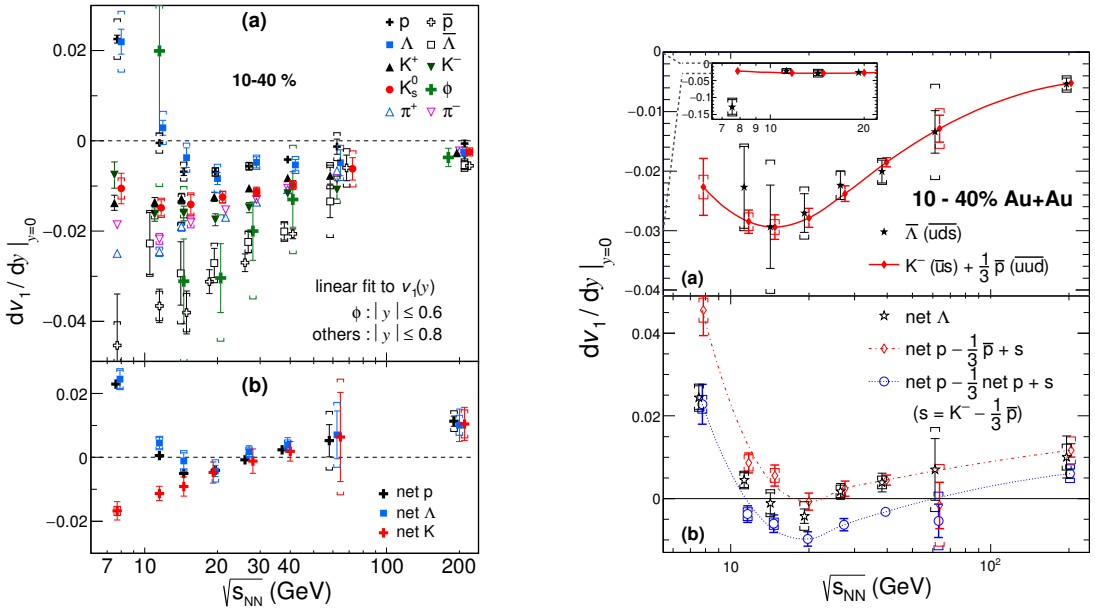

Figure 1. Left: Directed flow slope (dv_1/dy) versus beam energy for midcentral (10-40%) Au+Au collisions. Panel (a) presents (anti)protons, Λ, $\bar{\Lambda}$, ϕ meson, and kaons. Panel (b) shows net protons, net Λs and net kaons. Right: Directed flow slope (dv_1/dy) versus $\sqrt{s_{NN}}$ for midcentral (10-40%) collisions. Panel (a) compares the observed $\bar{\Lambda}$ slope with the expectation fromt the coalescence sum rule for produced quarks. Panel (b) shows test of the coalescence sum rule for net-Λ measurement.

The ten particle species were used for the investigation of the scaling behavior of v_1 at the constituent quark level versus collision energy [11,12]. In the test several assumptions have been made. First, v_1 is developed at the pre-hadronic stage. Second, specific quark types have the same directed flow. Third, the registered hadrons are formed via coalescence. In a scenario when deconfined quarks have acquired azimuthal anisotropy, and in the limit of small v_n, coalescence leads to the azimuthal anisotropy of the resulting mesons or baryons being the summed v_n of their constituent quarks. We call this the coalescence sum rule.

Firstly, the coalescence sum rule is tested in a scenario where all quarks are known to be produced. Figure 1(a)(right) shows a comparison of the observed dv_1/dy for $\bar{\Lambda}$ ($\bar{u}\bar{d}\bar{s}$) with

the calculation for $K^-(\bar{u}s) + \frac{1}{3}\bar{p}(\bar{u}\bar{u}\bar{d})$. This calculation is based on the coalescence sum rule combined with the assumption that $\bar{u}$ and $\bar{d}$ have the same flow, and that s and $\bar{s}$ have the same flow. A good agreement has been found for the energy range from 200 to 11.5 GeV, while a breakdown of agreement is found at $\sqrt{s_{NN}}$ =7.7 GeV (inset in Fig. 1(a)(right)). It implies that one or more assumptions are no longer hold below 11.5 GeV.

In the limit of low $\sqrt{s_{NN}}$, most u and d quarks are presumably transported, whereas in the limit of high $\sqrt{s_{NN}}$, most of u and d are produced. In Fig. 1(b)(right), we exploit net Λ (uds) to test two coalescence sum rule scenarios which are expected to bracket the observed dv_1/dy for a baryon containing transported quarks.

The first compared calculation (red diamond markers) consists of net proton (uud) minus $\bar{u}$ plus s, where $\bar{u}$ is estimated from $\frac{1}{3}\bar{p}$, and the s quark flow is obtained from $K^-(\bar{u}s) - \frac{1}{3}\bar{p}(\bar{u}\bar{u}\bar{d})$. Here we assume that a produced u quark in net p is replaced with an s quark. This sum-rule calculation agrees closely with the net-Λ measurement at $\sqrt{s_{NN}} = 19.6$ GeV and above, remains moderately close at 14.5 and 11.5 GeV, and has a significant deviation at 7.7 GeV. The fraction of transported quarks among the constituent quarks of net protons increases with decreasing beam energy, and there is an increasing departure from the assumption that a produced u quark is removed by keeping the term (net $p - \frac{1}{3}\bar{p}$).

The second coalescence calculation in Fig. 1(b)(right) corresponds to 2/3 net proton plus s (blue circle markers). In this case, we assume that the constituent quarks of net protons are dominated by transported quarks in the limit of low beam energy, and that one of the transported quarks is replaced by s. This approximation seems to hold at $\sqrt{s_{NN}} = 7.7$ GeV, and breaks at higher energies.

In case of the heavy quarks, it has been suggested that the magnitude of the rapidity-odd directed flow, v_1, for open charm hadrons is sensitive to the tilted shape of the initial source and to the charm quark drag coefficient in the QGP, while the difference in v_1 between charm and anti-charm hadrons is sensitive to the electromagnetic field in heavy-ion collisions [13, 14]. Using the HFT, STAR has found the first evidence of a non-zero v_1 for open charm hadrons in heavy-ion collisions. Figure 2 shows the results of D^0 v_1 measured in Au+Au collisions at $\sqrt{s_{NN}} = 200$ GeV.

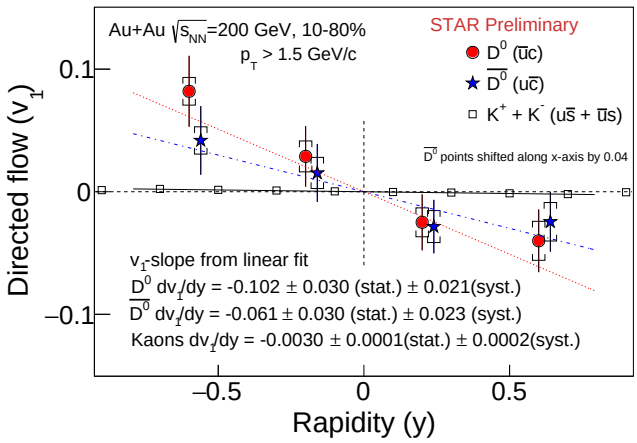

Figure 2. Directed flow, v_1, for D^0 (circles), $\bar{D}^0$ (stars) and $K^{\pm}$ (boxes) as a function of rapidity, y, in 10-80% Au+Au collisions at $\sqrt{s_{NN}} = 200$ GeV. Vertical bars (brackets) represent statistical (systematic) uncertainties. Lines represent linear fits to the data.

The v_1 slope at midrapidity (dv_1/dy), averaged for D^0 and $\bar{D}^0$ mesons, was extracted $dv_1/dy = -0.081 \pm 0.021_{(stat)} \pm 0.017_{(syst)}$, which is significantly larger that that of charged

kaons. The dv_1/dy values for the D^0 and $\bar{D}^0$ mesons are consistent with each other within uncertainties.

3. Flow decorrelations

Longitudinal decorrelations of flow harmonics are sensitive to event-by-event fluctuations of the initial-collision geometry and final-state collective dynamics. Using the FMS as the reference detector, STAR has measured longitudinal decorrelations from 2016 data in Au+Au collisions at $\sqrt{s_{NN}} = 200$ GeV. The factorization ratios r_2 and r_3 [15] are used to measure the decorrelation of v_2 and v_3, respectively, between η_a and -η_a in the pseudorapidity range $|\eta| < 1$, with respect to a common reference $2.5 < \eta_b < 4$. They are found to exhibit a stronger decrease with the normalized rapidity (η_a/y_{beam}) than those at the LHC [16], as can be seen in Fig. 3.

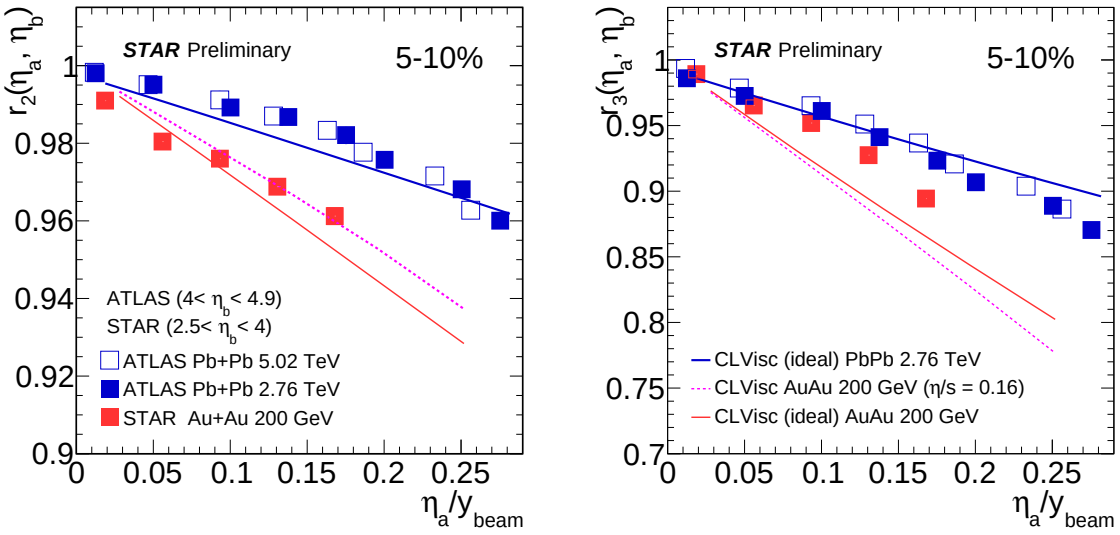

Figure 3. The factorization ratio r_n for v_2 (left plot) and v_3 (right plot) in 5-10% Au+Au collisions at $\sqrt{s_{NN}} = 200$ GeV (red filled boxes), Pb+Pb collisions at 2.76 and 5.02 TeV (blue filled and open boxes). Also shown are (3+1)D hydrodynamic calculations [17, 18].

This is qualitatively consistent with (3+1)D hydrodynamic calculations [17, 18]. However, these calculations can not simultaneously describe both the RHIC and LHC data. Analyses of data in Au+Au collisions at lower energies are underway to provide more insight into the decorrelations.

4. Di-hadron correlations

In heavy-ion collisions, two-body scatterings can occur with large momentum transfer. The scattered partons are created back-to-back and fragment into di-jet pairs. Jets lose their energy through interacting with the QGP and hence, jets can serve as a good probe of energy loss mechanisms in the medium. This can be studied via correlations of high-p_T triggered particles, as proxies for the jets, with associated particles as a function of the relative azimuthal angle. Since the evolution of a collision system is sensitive to fluctuations of the initial geometry of the participant region, event shape engineering (ESE) was proposed as a useful tool to select the initial geometry of the system utilizing the fluctuations of the magnitude of the flow vector q_2 [19]. The combination of centrality selection and ESE allows one to control the initial geometry while keeping the average energy density fixed.

Figure 4 shows the centrality dependence of mid-plane region ($-2\pi/8 < \phi^t - \Psi_2 < -\pi/8$) with large (magenta markers) and small (blue markers) q_2 selections for 0-10% (left panel), 10-40% (middle panel) and 40-60% (right panel) centrality classes.

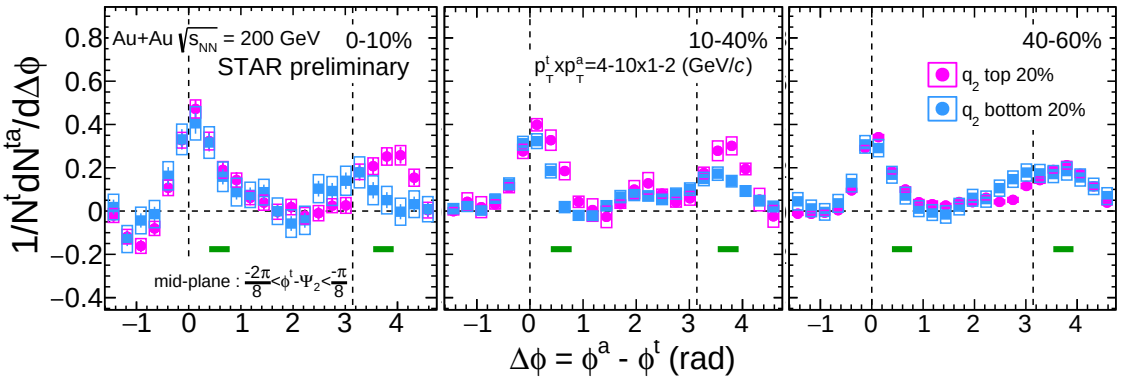

Figure 4. Di-hadron correlations with trigger angle selected to mid-plane ($-2\pi/8 < \phi^t - \Psi_2 < -\pi/8$) with respect to the second-order event plane with top-q_2 20% (magenta markers) and bottom-q_2 (blue markers) selections in 0-10% (left plot), 10-40% (middle plot) and 40-60% (right plot) centrality. The p_T range of the triggered particle is $4 < p_T^t < 10$ GeV/c and that of the associated particle is $1 < p_T^a < 2$ GeV/c. Statistical errors may be smaller than the symbol size, systematic uncertainties are indicated as colored boxes. The green bars at $y \approx -0.2$ indicate the event-plane directions.

Larger shifts of the away-side peak position are observed in large-q_2 events in 0-10% and 10-40% centralities and the difference is larger in central events, but no q_2 dependence is observed in 40-60% within systematic uncertainties. The difference in the shape of correlations between large-q_2 and small-q_2 events might be due to the difference in the strength of the elliptic flow, and the difference is larger in lower-p_T associated particles. This might be a hint of quenched jets coupled with the expanding medium.

5. Λ_c production

The Λ_c is the lightest baryon containing a charm quark. The Λ_c yield at intermediate transverse momentum is expected to be enhanced in heavy-ion collisions with respect to p+p collisions, in case charm quarks hadronize via coalescence similarly to light flavor quarks. In 2017 STAR presented the first result on the Λ_c production in heavy-ion collisions at the QM2017 conference, obtained from the 2014 data with the HFT in Au+Au collisions at $\sqrt{s_{NN}} = 200$ GeV. Adding the data from Au+Au collisions taken in 2016, and using a supervised machine-learning method based on boosted decision trees, the Λ_c signal significance is increased by a factor of two as compared to the previous study. Figure 5 shows the ratio of Λ_c/D^0 yields as a function of centrality (left panel) and p_T (right panel).

It is found that the Λ_c/D^0 ratio increases towards more central Au+Au collisions, and the ratio in peripheral Au+Au collisions is compatible with that in p+p collisions at $\sqrt{s} = 7$ TeV measured by ALICE [20]. The ratio, when plotted as a function of p_T and integrated over the 10-80% centrality interval, is much closer to theoretical calculations considering charm quark coalescence [21, 22] than the PYTHIA prediction in p+p collisions [23].

6. Global and local hyperon polarization

In non-central heavy-ion collisions, the created medium is supposed to have a large angular momentum transferred from the two colliding nuclei. As it was shown in Refs. [24, 25], such an

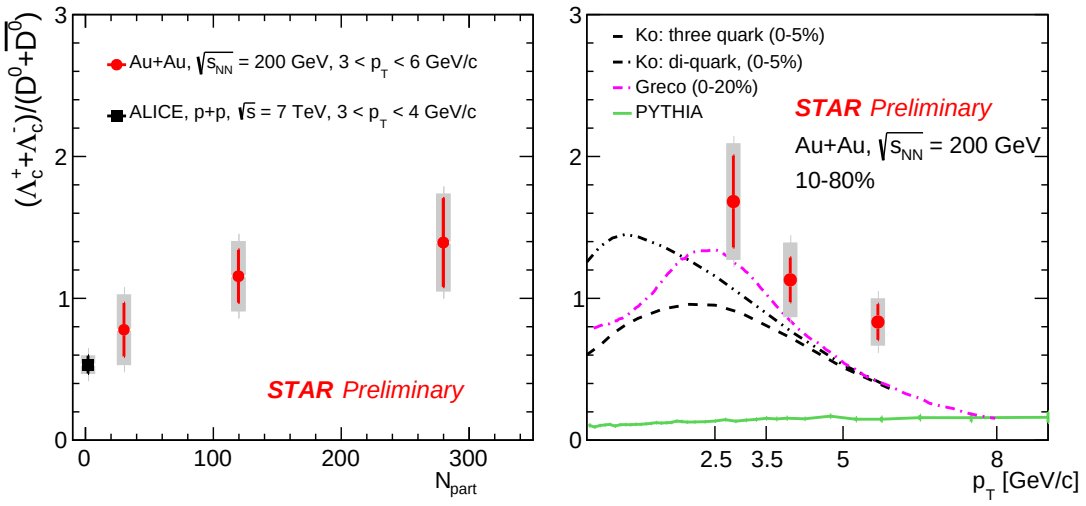

Figure 5. The Λ_c/D^0 ratio in Au+Au collisions at $\sqrt{s_{NN}} = 200$ GeV as a function of centrality (left panel) and p_T (right panel). Vertical bars (shaded areas) represent statistical (systematic) uncertainties. Also shown are the ratio in p+p collisions at $\sqrt{s} = 7$ TeV measured by ALICE (black box), PYTHIA prediction (solid curve), and theoretical model calculations including charm quark coalescence (other curves).

initial angular momentum would be partially transferred to the spin of produced particles and then the resulting global polarization would be experimentally detectable via hyperons through their parity-violating weak decays.

The first global polarization measurements were performed by STAR using Λ hyperons at $\sqrt{s_{NN}} = 62.4$ and 200 GeV, where the signal was consistent with zero [26]. Later [27], STAR has observed non-zero positive signals of hyperon global polarization in Au+Au collisions at $\sqrt{s_{NN}} = 7.7$–39 GeV with a possible difference between Λ and $\bar{\Lambda}$ that may arise from the initial magnetic field. Figure 6 (left panel) shows the results of the global Λ polarization for 20-50% centrality as a function of collision energy [28]. The red and blue stars show the measured Λ for Au+Au collisions at $\sqrt{s_{NN}} = 200$ GeV with the combined data from 2010, 2011 and 2014 years. These new results for 200 GeV show non-zero positive signals for both Λ and $\bar{\Lambda}$. This confirms that the polarization decreases with increasing collision energy, by comparing with the results from lower energies.

The initial angular momentum of the medium provides an average direction of the vorticity and therefore the particle polarization, however the vorticity can be locally non-zero as well. As discussed in Refs. [32, 33], a local vorticity along the beam direction may be created due to the presence of elliptic flow. Similar to the global polarization, the polarization projected onto the beam direction, P_z, can be written as:

$$P_z = \frac{\langle \cos\theta_p^* \rangle}{\alpha_H \langle (\cos\theta_p^*)^2 \rangle}, \tag{2}$$

where θ_p^* is the polar angle of daughter proton in the Λ rest frame. The subscript H denotes Λ or $\bar{\Lambda}$, and the decay parameter $\alpha_\Lambda = -\alpha_{\bar{\Lambda}} = 0.642 \pm 0.013$ [34]. Figure 6 (right panel) shows $< \cos\theta_p^* >$ as a function of azimuthal angle relative to the second-order event plane. The data clearly shows a sine structure for both Λ and $\bar{\Lambda}$ as expected from the elliptic flow.

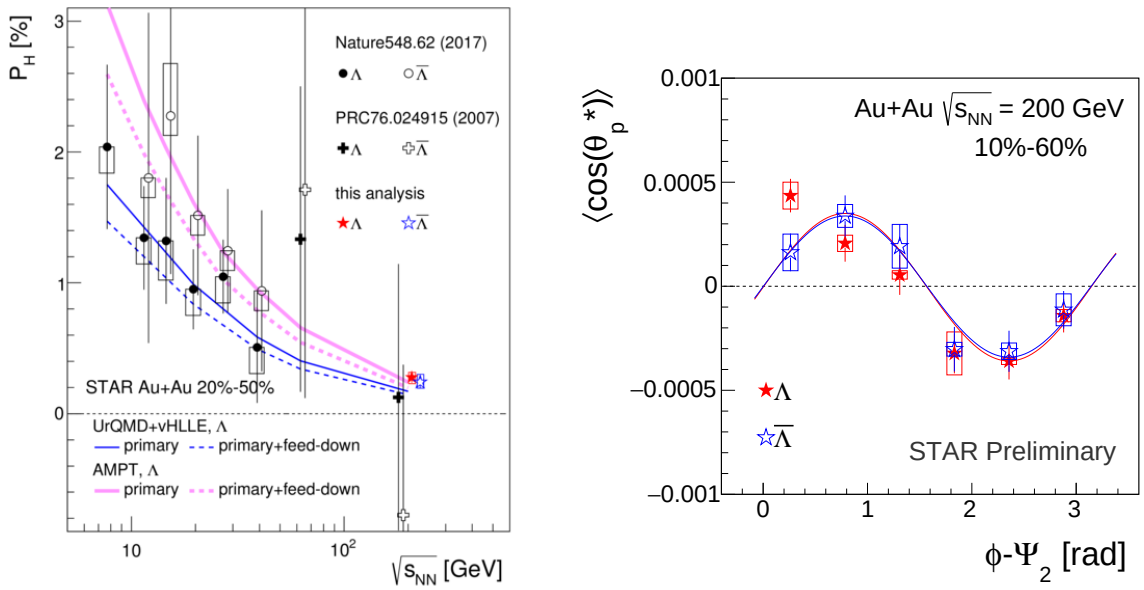

Figure 6. (Left panel) Global polarization of Λ and $\bar{\Lambda}$ as a function of the collision energy $\sqrt{s_{NN}}$ for 20-50% centrality Au+Au collisions. Thin lines show calculations from a (3+1)D cascade + viscous hydrodynamic model (UrQMD+vHLLE) [29] and bold lines show the AMPT model calculations [30]. In the case of each model, primary Λ with and without the feed-down effect [31] are indicated by dashed and solid lines, respectively. (Right panel) $< \cos\theta^*_p >$ of Λ and $\bar{\Lambda}$ as a function of hyperons' azimuthal angle, ϕ, relative to the second-order event plane angle Ψ_2 for 10-60% centrality bin in Au+Au collisions at $\sqrt{s_{NN}} = 200$ GeV. Resolution on Ψ_2 is not corrected.

7. Correlation femtoscopy

Two-particle interferometry measurement, known as femtoscopy or HBT, is a standard method of studying space and time characteristics of the created system in heavy-ion collisions [35]. It has been most common to perform the femtoscopic analyses with pions [36, 37] as they are the most abundantly produced particles in heavy-ion collisions. Data collected in the BES program allow measurements with the heavier but less abundant particles - kaons. In addition to the identification via specific ionization energy loss (dE/dx) in the TPC, the time-of-flight information from the TOF detector was used to identify pion and kaons. This allowed to perform particle identification in a wide momentum range of $0.15 \leq p$ (GeV/c)≤ 1.45.

Figure 7 shows the centrality and transverse mass ($m_T = \sqrt{k_T^2 + m^2}$, where $k_T = 0.5(p_{1,T} + p_{2,T})$) dependence of the extracted femtoscopic parameters λ, R_{out}, R_{side}, R_{long} and R_{out}/R_{side} for Au+Au collisions at $\sqrt{s_{NN}} = 39$ GeV. Similar measurements have been performed for other collision energies. While the transverse flow and expansion of the system are encoded in the falling of R_{out} and R_{side} with increasing m_T, the longitudinal flow exhibits a decrease of R_{long} with the increasing m_T. Such a behavior of source radii R_{out}, R_{side} and R_{long} confirms our expectation that the system under study undergoes space-time evolution and expands. The extracted R_{out} and R_{long} values for kaons are generally larger than those for pions at the same transverse mass, while R_{side} values for pion and kaons are similar.

In 2015 STAR conducted a Au+Au $\sqrt{s_{NN}} = 4.5$ GeV fixed-target test run to demonstrate STAR's capabilities in a fixed-target configuration. One beam was circulated in the collider and lowered to directly graze the edge of a 1 mm thick (4% interaction probability) gold foil

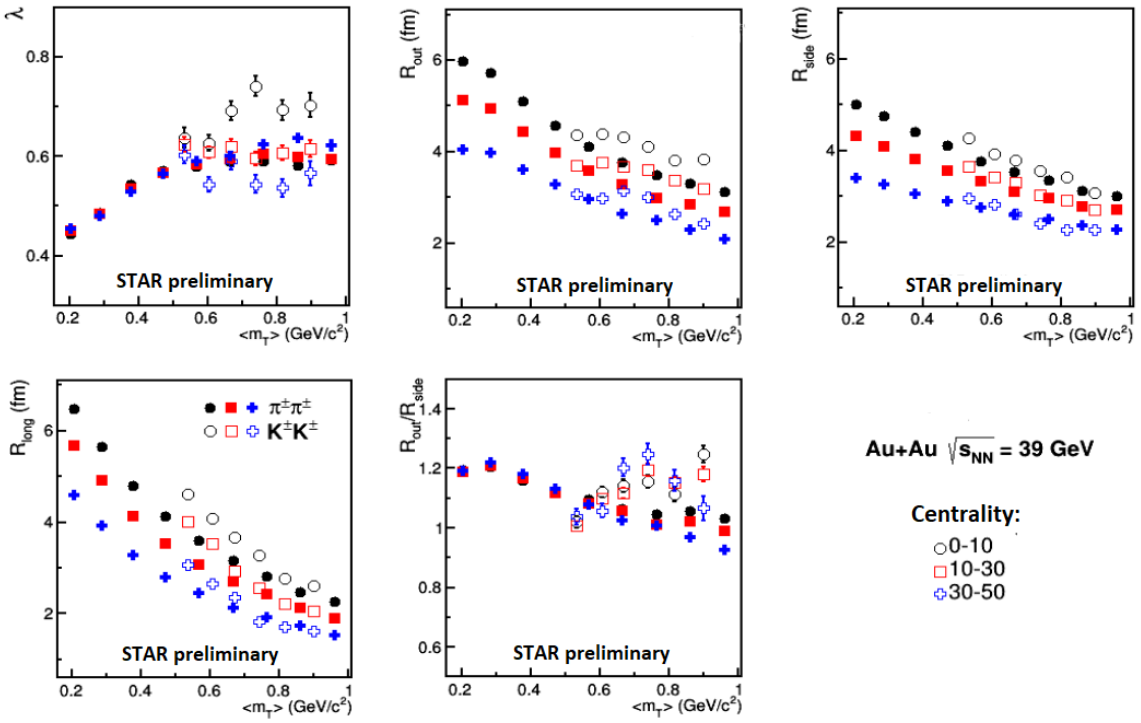

Figure 7. Transverse mass dependence of λ, R_{out}, R_{side}, R_{long} and R_{out}/R_{side} for pions (solid symbols) and kaons (open symbols) measured for 0–10% (circles), 10–30% (squares), and 30–50% (crosses) most central Au+Au collisions at $\sqrt{s_{NN}} = 39$ GeV. Only statistical uncertainties shown.

target. The target was placed at the edge of the TPC, about 211 cm away from the center of the detector to make use of the full tracking volume of the TPC. Approximately 1.3 million events were collected with a top $\approx 30\%$ centrality trigger. Figure 8 shows the measured femtoscopic radii as a function of transverse mass for 0-10% central Au+Au collisions in the fixed-target mode.

The STAR FXT results are compared with E895 [38] and E866 (E802) [39] and are consistent with the energy dependence trend of these other experiments within uncertainties.

8. Summary and Outlook

In 2018 STAR took data in Ru+Ru and Zr+Zr collisions to study the chiral magnetic effect, and Au+Au collisions at $\sqrt{s_{NN}} = 27$ GeV to look for difference in the global polarization between Λ and $\bar{\Lambda}$ due to the initial magnetic field. In 2019-2021, STAR will take data in both collider and fixed-target modes at $\sqrt{s_{NN}} = 3.0$–19.6 GeV to look for signatures of the critical point and phase transition of the QCD phase diagram, with new detectors including inner TPC, endcap TOF, and event plane detector for improved acceptance, particle identification and event plane reconstruction. STAR is also working on R&D for new forward calorimeter and tracking systems ($2.5 < \eta < 4$) for detailed studies of the initial conditions, longitudinal decorrelation and rapidity dependence of Λ global polarization in A+A collisions, and the partonic and spin structure of the nucleon and nuclei in p+p and p+A collisions in 2021+.

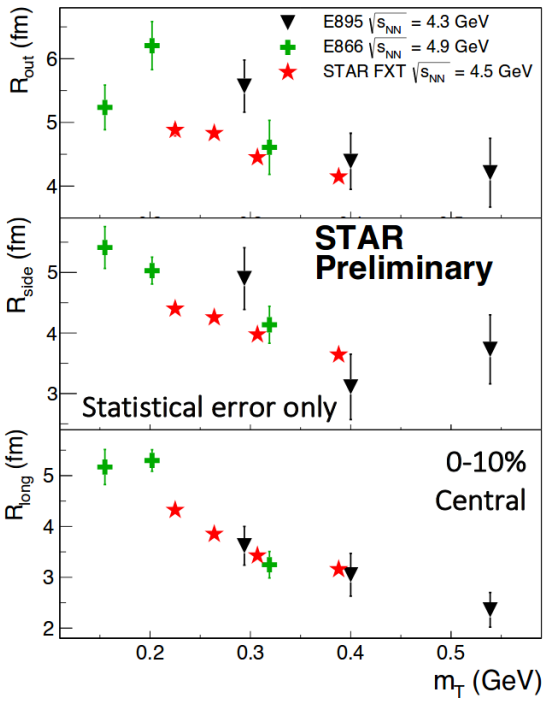

Figure 8. Transverse mass dependence of R_{out}, R_{side}, and R_{long} for pions measured for 0-10% Au+Au collisions in STAR (red stars), E895 (black triangles) [38], and E866 (green crosses) [39]. Only statistical uncertainties shown.

Acknowledgements

The reported study was funded by RFBR according to the research project No. 16-02-01119 a, supported by program of increasing the competitive ability of NRNU MEPhI (agreement with RMHES of August 27, 2013, project no. 02.a03.21.0005), and was partially supported by the Ministry of Science and Higher Education of the Russian Federation, grant N 3.3380.2017/4.6.

References

[1] Karsch F 2007 *Nucl. Phys. A* **783** 13
[2] Karsch F *et al.* 2004 *Nucl. Phys. B Proc. Suppl.* **129** 614
[3] Aoki Y, Endrodi G, Fodor Z, Katz S D and Szabo K K 2006 *Nature* **443** 675
[4] Ejiri S 2008 *Phys. Rev. D* **78** 074507
[5] Bowman E S and Kapusta J I 2009 *Phys. Rev. C* **79** 015202
[6] Adamczyk L *et al.* (*Preprint* 1007.2613)
[7] Voloshin S and Zhang Y 1996 *Z. Phys. C* **70** 665
[8] Poskanzer A M and Voloshin S A 1998 *Phys. Rev. C* **58** 1671
[9] Rischke D H *et al.* 1995 *Heavy Ion Phys.* **1** 309
[10] Stöcker H 2005 *Nucl. Phys. A* **750** 121
[11] Adamczyk L *et al.* 2014 *Phys. Rev. Lett.* **112** 162301
[12] Adamczyk L *et al.* 2018 *Phys. Rev. Lett.* **120** 062301
[13] Chatterjee S and Bozek P 2018 *Phys. Rev. Lett.* **120** 192301
[14] Das S *et al.* 2017 *Phys. Lett. B* **768** 260
[15] Khachatryan V *et al.* 2015 *Phys. Rev. C* **92** 034911
[16] Aaboud M *et al.* 2018 *Eur. Phys. J. C* **78** 142
[17] Pang L G *et al.* 2015 *Phys. Rev. D* **91** 074207
[18] Pang L G, Petersen H and Wang X N 2018 *Phys. Rev. C* **97** 064918
[19] Schukraft J, Timmins A and Voloshin S A 2013 *Phys. Lett. B* **719** 394
[20] Acharya S *et al.* 2018 *JHEP* **04** 108
[21] Lee S H *et al.* 2008 *Phys. Rev. Lett.* **100** 222301
[22] Ghosh S *et al.* 2014 *Phys. Rev. D* **90** 054018
[23] Sjöstrand T, Mrenna S and Skands P 2006 *JHEP* **026** 1
[24] Liang Z T and Wang X N 2005 *Phys. Rev. Lett.* **94** 102301
[25] Voloshin S A (*Preprint* 041008)

[26] Abelev B *et al.* 2007 *Phys. Rev. C* **76** 024915
[27] Adamczyk L *et al.* 2017 *Nature* **548** 62
[28] Adamczyk L *et al.* 2018 *Phys. Rev. C* **98** 014910
[29] Karpenko I and Becattini F 2017 *Eur. Phys. J. C* **77** 21
[30] Li H, Pang L G, Wang Q and Xia X L 2017 *Phys. Rev. C* **96** 054908
[31] Becattini F, Karpenko I, Lisa M, Upsal I and Voloshin S 2017 *Phys. Rev. C* **95** 054902
[32] Becattini F and Karpenko I 2018 *Phys. Rev. Lett.* **120** 012302
[33] Voloshin S A 2018 *EPJ Web Conf.* **17** 10700
[34] Olive K A *et al.* 2014 *Chin. Phys. C* **38** 090001
[35] Lisa M A, Pratt S, Soltz R and Wiedemann U 2005 *Ann. Rev. Nucl. Part. Sci.* **55** 357
[36] Adams J *et al.* 2005 *Phys. Rev. C* **71** 044906
[37] Adamczyk L *et al.* 2015 *Phys. Rev. C* **92** 014904
[38] Lisa M A *et al.* 2000 *Phys. Rev. Lett.* **84** 2798
[39] Ahle L *et al.* 2002 *Phys. Rev. C* **66** 054906